

瘤内联合瘤周影像组学预测乳腺癌新辅助治疗疗效的研究

王一如, 王海波*

青岛大学附属医院乳腺病诊疗中心, 山东 青岛

收稿日期: 2026年4月29日; 录用日期: 2026年5月23日; 发布日期: 2026年6月2日

摘要

研究目的: 本研究旨在通过融合动态对比增强磁共振成像(dynamic contrast-enhanced magnetic resonance imaging, DCE-MRI)的瘤内与瘤周影像组学特征, 开发并验证一种无创预测乳腺癌患者新辅助治疗(neoadjuvant systemic therapy, NST)后病理完全缓解(pathological complete response, pCR)状态的工具。**研究方法:** 回顾性分析534名乳腺癌患者的病理及影像资料。融合瘤内与瘤周3 mm特征构建联合预测模型, 与单纯瘤内模型进行比较。最后在训练集与验证集中计算曲线下面积(area under the curve, AUC)量化区分度; 绘制校准曲线评价模型预测概率与实际发生概率的一致性; 最后进行决策曲线分析(decision curve analysis, DCA), 在不同阈值概率范围内计算净获益, 以评估模型的潜在临床实用性。**主要结果:** 研究发现联合模型预测pCR的效能优于单纯瘤内模型。在验证集中, 其曲线下面积AUC达到0.851 (95% CI: 0.792~0.910), 优于单一瘤内模型0.840 (95% CI: 0.779~0.901)。此外, 在校准性能方面, 联合模型在训练集和验证集中均表现出良好的拟合度; DCA证实, 该模型在临床决策分析中显示出较高的净获益。**结论:** 本研究证实结合瘤内、瘤周信息特征的联合模型能精准预测乳腺癌NST的疗效。该模型在判别能力、校准性能和临床实用性方面均表现优越, 可作为治疗前个体化疗效预测的候选工具。但本研究为回顾性单中心设计, 研究结果尚需前瞻性多中心外部验证。

关键词

乳腺癌, 新辅助治疗, 磁共振成像, 影像组学

A Study on Intratumoral and Peritumoral Radiomics for Predicting the Response to Neoadjuvant Therapy in Breast Cancer

Yiru Wang, Haibo Wang*

Department of Breast Diagnosis and Treatment Center, The Affiliated Hospital of Qingdao University, Qingdao Shandong

*通讯作者。

Abstract

Objective: This study aimed to develop and validate a noninvasive tool for predicting pathological complete response (pCR) after neoadjuvant systemic therapy (NST) in breast cancer patients, by integrating intratumoral and peritumoral radiomic features derived from dynamic contrast-enhanced magnetic resonance imaging (DCE-MRI). **Methods:** A total of 534 breast cancer patients were retrospectively enrolled, and their clinical pathological and imaging data were analyzed. A combined prediction model was constructed by integrating intratumoral features and 3-mm peritumoral radiomic features, which was further compared with the single intratumoral model. The area under the curve (AUC) was calculated in the training and validation cohorts to quantify the discriminative ability of models. Calibration curves were plotted to assess the consistency between predicted probability and actual probability. Decision curve analysis (DCA) was performed to calculate the net clinical benefit across different threshold probabilities, so as to evaluate the clinical application value of the model. **Results:** The combined model yielded better predictive performance for pCR than the single intratumoral model. In the validation cohort, the combined model achieved an AUC of 0.851 (95% CI: 0.792~0.910), superior to 0.840 (95% CI: 0.779~0.901) of the single intratumoral model. Moreover, the combined model presented favorable calibration goodness-of-fit in both training and validation sets. DCA demonstrated that the combined model provided higher net clinical benefit for clinical decision-making. **Conclusion:** The combined model integrating intratumoral and peritumoral radiomic features can accurately predict NST response in breast cancer. It exhibits excellent performance in discrimination, calibration and clinical practicability, which can serve as a promising candidate tool for individualized pretreatment efficacy prediction. Nevertheless, this study is a retrospective single-center research, and further prospective multicenter external validation is required to confirm the generalizability of the findings.

Keywords

Breast Cancer, Neoadjuvant Therapy, Magnetic Resonance Imaging, Radiomics

Copyright © 2026 by author(s) and Hans Publishers Inc.

This work is licensed under the Creative Commons Attribution International License (CC BY 4.0).

<http://creativecommons.org/licenses/by/4.0/>



Open Access

1. 绪论

乳腺癌作为全球女性最常见的恶性肿瘤之一, 具有高度的侵袭性和治疗复杂性, 据 GLOBOCAN 2022 统计数据显示, 全球每年新发乳腺癌约 230 万例, 死亡约 67 万例, 严重威胁女性的生命健康[1]。

新辅助治疗(neoadjuvant systemic therapy, NST)是局部晚期乳腺癌治疗的标准策略, 其核心在于缩减肿瘤体积、实现临床降期以提高保乳率, 同时为体内药敏评估提供窗口期。在 NST 后达到病理完全缓解(pathological complete response, pCR), 已成为评估乳腺癌疗效及预测长期预后的关键替代终点。CTNeoBC 荟萃分析及 I-SPY 2 系列研究均证实, 达到 pCR 的患者在无事件生存期和总生存期方面显著优于未达到 pCR 者, 这种差异在三阴性乳腺癌和人表皮生长因子受体 2 (human epidermal growth factor receptor 2, HER-2)阳性亚型中尤为显著[2] [3]。然而, 现有研究结果表明接受 NST 的患者中仅约 15%~40%能够达到 pCR, 且约 5%的患者在治疗过程中出现疾病进展[4]。因此, 早期、准确地预测 NST 疗效, 对于实现个体化精

准治疗决策至关重要。

在现有影像学评估手段中, 动态对比增强磁共振成像(dynamic contrast-enhanced magnetic resonance imaging, DCE-MRI)凭借对肿瘤形态学参数(如体积、大小)及血流动力学参数(如 K^{trans} 、 K_{ep})的定量分析能力, 已成为评估 NST 疗效与残留病灶的标准影像学工具。然而, 其在临床应用中存在明显局限。其疗效评估依赖半定量分析与医师主观判断, 诊断稳定性不足; 同时肿瘤微环境改变及化疗相关效应易造成病灶评估偏差, 共同导致其难以精准评价 NST 疗效[5]。

影像组学为解决上述问题提供了新的技术路径。该概念由 Lambin 等首次提出[6], 其核心思想是借助计算机算法从医学影像中高容量提取肉眼难以识别的定量特征(包括形态、纹理、滤波变换特征等), 并利用机器学习进行分析, 从而将影像信息转化为可量化、可挖掘的高维数据。目前, MRI 影像组学在乳腺癌的鉴别诊断[7]-[9]、分子亚型分析[10][11]、淋巴结转移预测[12]-[14]及新辅助治疗疗效评估[15][16]中已展现出显著的应用潜力。

值得注意的是, 肿瘤并非孤立存在的实体。肿瘤微环境在肿瘤发生、进展及转移过程中发挥关键的调控作用, 其中免疫细胞浸润、血管生成和纤维化反应在治疗中扮演重要角色[17]-[19]。将瘤周定量影像特征纳入分析框架, 有望捕获瘤内特征无法反映的微环境信息, 提升 pCR 预测准确性。

综上所述, 本研究拟以接受 NST 的乳腺癌患者治疗前 DCE-MRI 图像为研究对象, 联合瘤内区域与瘤周 3 mm 区域提取定量影像组学特征, 结合机器学习方法构建 pCR 预测模型并评估其预测效能, 以期成为乳腺癌患者的个体化精准治疗决策提供无创、客观的影像学工具。

2. 材料与方法

2.1. 数据采集

收集 2021 年 1 月至 2023 年 12 月期间在我院经穿刺活检确诊乳腺癌并完成新辅助治疗及手术的患者临床及影像资料进行回顾性分析(流程图见图 1)。纳入标准如下: (1) 单侧原发非特殊类型浸润性乳腺癌(病理确诊); (2) NST 前完成完整乳腺 MRI 检查且图像质量合格; (3) 完整病理资料(治疗前、后); (4) NST 前未接受其他抗肿瘤治疗。排除标准如下: (1) MRI 图像质量无法分析; (2) 资料缺失; (3) 既往乳腺手术或放疗史; (4) 双侧乳腺癌、隐匿性乳腺癌或远处转移; (5) 其他恶性肿瘤史; (6) 未接受标准 NST 方案; (7) 病灶过小或边界不清, 难以准确勾画感兴趣区域(region of interest, ROI)。

最终纳入 534 名患者, 按 7:3 比例随机分为训练集与验证集, 统计学验证了组间基线数据平衡。

收集临床及病理特征包括: 年龄、月经状态、BMI、TNM 分期、肿瘤最大径、雌激素受体(estrogen receptor, ER)、孕激素受体(progesterone receptor, PR)、HER-2、Ki-67、淋巴结状态、Miller-Payne 分级等。判读标准如下: ER/PR: $\geq 1\%$ 染色为阳性, $< 1\%$ 为阴性[20]; HER-2: HER-2 阳性的判读结果为 3+, 0 或 1+则被判读为阴性, 当为 2+时, 需要荧光原位杂交技术确定, 若扩增则判读为阳性, 否则为阴性[21]。

所有患者均接受标准 NST 方案(蒽环类 + 紫杉类为基础, HER-2 阳性者联合靶向治疗, 部分激素受体阳性者辅以内分泌治疗) [22]。本研究以 pCR 作为 NST 的疗效评价指标, 定义为乳腺原发病灶及区域淋巴结内无浸润性癌残留(允许存在原位癌) [23]。本研究聚焦于评估瘤内联合瘤周影像组学模型的独立预测价值, 临床基线数据仅用于描述研究人群及验证数据划分的均衡性, 未纳入模型构建。

2.2. MRI 数据采集

所有纳入患者在 NST 开始前 1~2 周内, 采用 3.0 T MRI 扫描仪(GE Signa HDxt)配合专用 16 通道乳腺线圈完成基线扫描。患者均取俯卧位, 以确保双侧乳腺自然悬垂。动态增强扫描包含 1 期脂肪抑制的 T1 加权成像及 8 期增强扫描。对比剂使用 Gd-DTPA (0.1 ml/kg), 经静脉以 2 ml/s 流速推注。首期增强扫

描在注药后 60 s 开始, 后续连续采集 7 期, 单期扫描时间约 65 s。主要参数见表 1。所有原始影像以 DICOM 格式从医院 PACS 系统中导出。由两名资深放射科医生对图像质量进行严格筛查, 剔除存在显著运动伪影或图像失真、不满足影像组学分析要求的病例。

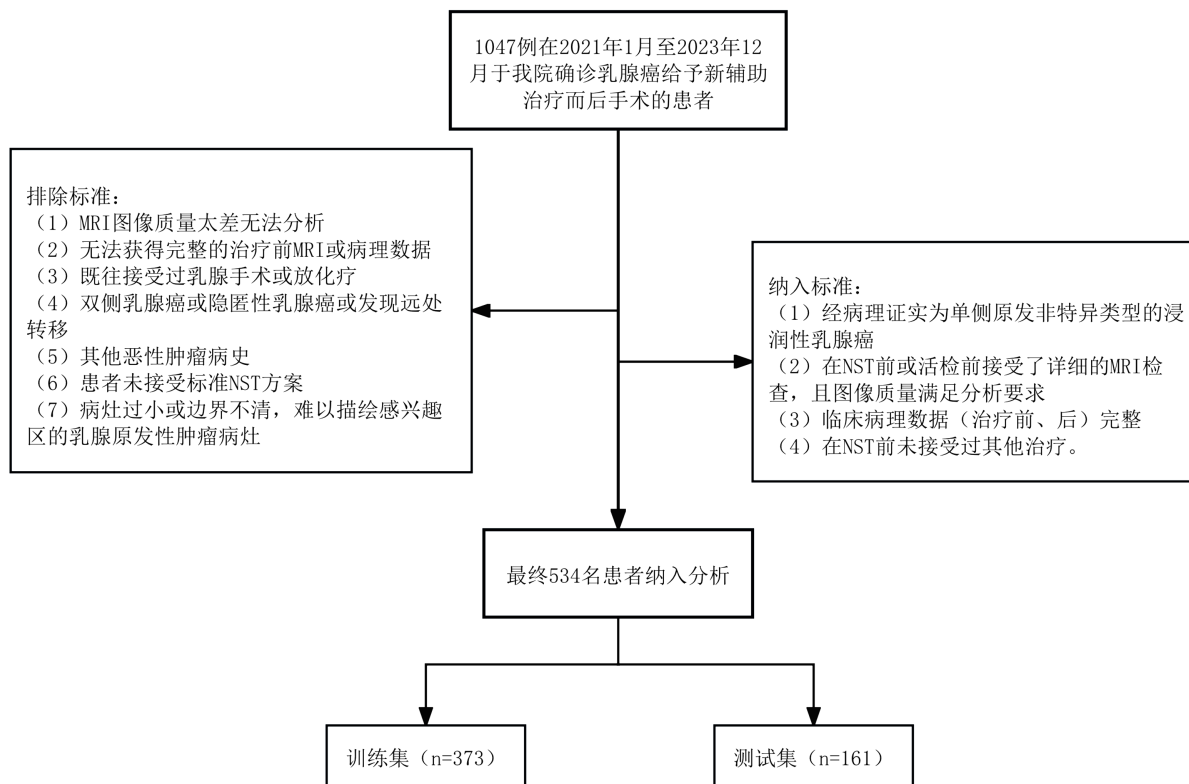


Figure 1. Recruitment pathways of researchers
图 1. 研究人员入组途径

Table 1. DCE-MRI scanning parameters
表 1. DCE-MRI 扫描参数

参数	数值
重复时间	4.25 ms
回波时间	2.1 ms
层厚	0.7 mm
层间距	1.5 mm
采集矩阵	320 × 320
视野	380 × 380 mm

2.3. 感兴趣区域定义与分割

为提升特征提取的可靠性, 本研究选择病灶强化最显著的增强早期(第一期)进行分析。在分割前对原始图像进行标准化处理: 采用 N4 偏置场算法消除磁场不均匀导致的信号失真; 随后通过固定分辨率重采样, 将体素统一为各向同性的 $1 \times 1 \times 1 \text{ mm}^3$, 以消除空间分辨率差异带来的偏移; 最后, 采用 Z-Score 标准化对灰度强度分布进行标准化处理, 以此保证不同患者队列间的信号特征具有可比性。

由两名具备十年以上临床经验的资深放射科医师以双盲法独立完成肿瘤分割, 全程操作严谨规范。基于 ITK-SNAP 软件(4.2 版本), 对肿瘤边界进行逐层手动勾画。对于多灶性病变患者, 仅选取直径最大的单一病灶纳入分析。最终由一名拥有二十年临床经验的权威影像专家对所有初步分割结果复核确认后, 确定三维感兴趣体积(volume of interest, VOI)。为评估分割可重复性, 两名放射科医师在训练集中随机抽取的 50 例样本进行独立分割, 在训练集内计算组内相关系数(intraclass correlation coefficient, ICC), 评估影像组学特征对分割差异的稳健性, 仅保留 $ICC \geq 0.75$ 的稳健特征, 用于后续特征筛选与建模。该设计确保基于可重复性的特征筛选仅在训练集内完成, 避免向验证集产生信息泄露。

Braman 等[24]率先将瘤周影像组学应用于乳腺癌 pCR 预测, 基于 117 例患者构建的瘤内 - 瘤周联合模型在训练集与验证集中 AUC 分别达 0.78 ± 0.03 和 0.74, 初步验证了瘤周区域的预测价值。该团队后续在 HER-2 阳性乳腺癌中进一步开展影像 - 病理关联分析[25], 结果显示 0~3 mm 瘤周区域的 Gabor 特征与肿瘤浸润淋巴细胞密度高度相关, 表明该范围内的影像学特征能够有效映射瘤周免疫微环境状态。基于此, 本研究利用 Python 3.7 软件, 将手动分割的 ROI 分别向外自动扩展 3 mm 以构建瘤周区域。对所有瘤周感兴趣区域进行人工核查, 剔除皮肤、乳头、胸壁肌肉及乳腺实质外的非腺体组织。上述处理流程保障了后续特征提取的准确性, 具体流程示意图见图 2。

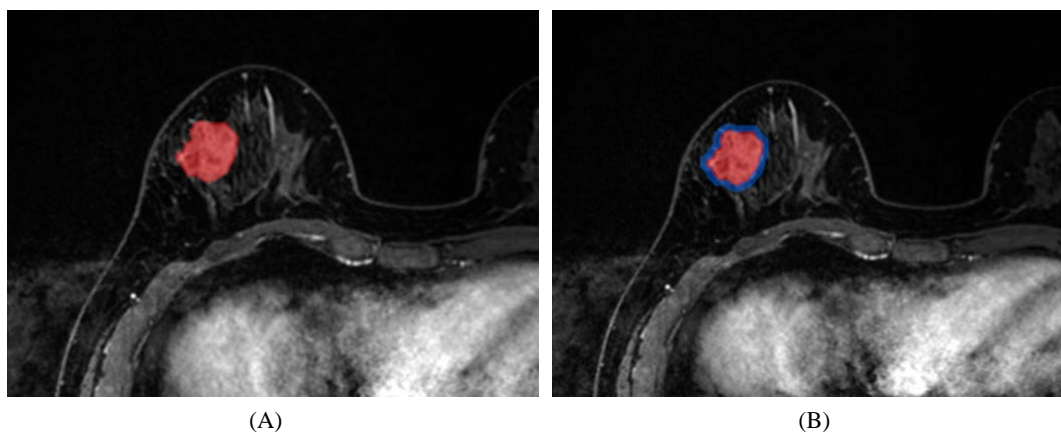


Figure 2. Schematic diagram of intratumoral and peritumoral ROI segmentation. (A) Intratumoral region; (B) Intratumoral and peritumoral 3 mm region

图 2. 肿瘤内和肿瘤周围 ROI 分割示意图。(A) 瘤内区域; (B) 瘤内 + 瘤周 3 mm 区域

2.4. 影像组学特征提取

基于 PyRadiomics 3.1, 从原始图像、小波变换(wavelet transformation)图像及高斯拉普拉斯滤波(Laplacian of Gaussian, LoG)图像中高通量提取影像组学特征。提取的特征类别包括形态特征、一阶统计特征(first-order statistical features), 以及基于灰度共生矩阵(gray-level co-occurrence matrix, GLCM)、灰度依赖矩阵(gray-level dependence matrix, GLDM)、灰度游程矩阵(gray-level run-length matrix, GLRLM)、灰度区域大小矩阵(gray-level size zone matrix, GLSZM)和邻域灰度差矩阵(neighboring gray-level dependence matrix, NGLDM)的纹理特征。

2.5. 特征筛选与降维

本研究提取的传统影像组学特征数量庞大, 远超样本量, 且存在大量相关性强、冗余或无关的特征。若直接全部输入模型, 极易导致过拟合, 降低泛化能力和鲁棒性[22] [23] [26] [27]。

所有变量筛选与降维过程均仅在训练集内部完成, 严格隔离验证集数据, 以保证实验严谨性。首先

采用独立样本 t 检验与 Mann-Whitney U 检验进行初步筛选, 保留 pCR 组与非 pCR 组间差异具有统计学意义($P < 0.05$)的特征。为减轻多重共线性问题, 采用 Spearman 相关性分析, 剔除相关系数绝对值 $|\rho| > 0.90$ 的冗余变量, 降低特征空间维数。最终采用最小绝对收敛和选择算子(Least Absolute Shrinkage and Selection Operator, LASSO)算法完成特征筛选。该 L1 正则化方法可自动将无关变量的系数压缩至 0, 通过十折交叉验证确定最优惩罚系数(λ), 最终仅保留系数非零的特征用于构建模型。

2.6. 影像组学模型构建、优化策略与评价指标

为避免单一算法的偶然性结果, 本研究采用四种机器学习算法进行对比验证, 包括逻辑回归(logistic regression, LR)、随机森林(random forest, RF)、支持向量机(support vector machine, SVM)与极端梯度提升(eXtreme Gradient Boosting, XGBoost)。

所有模型均采用标准化、无偏倚的建模流程。在训练集内执行五折分层交叉验证, 并结合网格搜索进行超参数优化。为解决类别不平衡问题, 在五折交叉验证过程中, 仅在每一折的训练子集内使用合成少数类过采样技术, 确保合成样本仅来源于训练数据, 不污染测试子集与独立验证集。预处理参数(如标准化)亦仅在训练集上完成调优, 严格避免信息泄露。采用受试者工作特征(Receiver Operating Characteristic, ROC)曲线及曲线下面积(area under the curve, AUC)、准确率、灵敏度、特异度、F1 分数等指标量化模型性能。采用校准曲线评估模型预测值与实际值的一致性。通过决策曲线分析(decision curve analysis, DCA)计算不同阈值概率下的净获益, 评估模型的临床适用性。

2.7. 统计分析

所有计算流程与统计分析均基于 Python 3.7 及 statsmodels 软件包完成。连续变量依据分布类型选择统计方法: 符合正态分布者采用独立样本 t 检验(以均值 \pm 标准差表示), 偏态分布者采用 Mann-Whitney U 检验(以中位数和四分位距表示)。分类变量则根据适用情况采用卡方检验或 Fisher 精确检验进行组间率的比较。所有比较均以 $P < 0.05$ 为差异具有统计学意义。

3. 结果

3.1. 样本分布与组间平衡

本研究纳入 534 例患者, 总 pCR 率为 31.5% (168/534), 非 pCR 率为 68.5% (366/534)。样本按 7:3 比例随机分为训练集($n = 373$, pCR 率 30.6%)和验证集($n = 161$, pCR 率 33.5%), 两组 pCR 比例接近, 基线特征无显著差异(均 $P > 0.05$), 确保了数据集拆分的合理性(表 2)。

Table 2. Baseline characteristics

表 2. 基线特征

特征	全部数据	训练集(n = 373)			全部数据	验证集(n = 161)			P 值 [†]
		Non-pCR (n = 259)	pCR (n = 114)	P 值*		Non-pCR (n = 107)	pCR (n = 54)	P 值*	
年龄(岁)	51.04 \pm 10.09	51.28 \pm 10.23	50.51 \pm 9.81	0.522	50.89 \pm 13.54	50.48 \pm 10.29	51.72 \pm 18.46	0.880	0.398
BMI (kg/m ²)	25.14 \pm 3.68	25.46 \pm 3.80	24.43 \pm 3.30	0.021	25.03 \pm 2.99	25.44 \pm 2.75	24.23 \pm 3.30	0.15	0.790
Ki-67	0.40 (0.20~0.60)	0.30 (0.20~0.50)	0.40 (0.30~0.70)	<0.001	0.40 (0.20~0.60)	0.4 (0.20~0.50)	0.40 (0.30~0.60)	0.024	0.673
肿瘤最大 直径(mm)	48.97 \pm 22.30	49.14 \pm 22.49	48.57 \pm 21.97	0.907	47.10 \pm 23.05	46.81 \pm 21.07	47.67 \pm 26.74	0.781	0.269

续表

月经状态				0.742				0.739	0.297
未绝经	170 (45.6)	120 (46.3)	50 (43.9)		82 (50.9)	53 (49.5)	29 (53.7)		
绝经	203 (54.4)	139 (53.7)	64 (56.1)		79 (49.0)	54 (50.5)	25 (46.3)		
T 分期				0.445				0.246	0.282
1	19 (5.1)	10 (3.9)	9 (7.9)		14 (8.7)	6 (5.6)	8 (14.8)		
2	190 (50.9)	134 (51.7)	56 (49.1)		84 (52.2)	57 (53.3)	27 (50.0)		
3	144 (38.6)	101 (39.0)	43 (37.7)		58 (36.0)	40 (37.4)	18 (33.3)		
4	20 (5.4)	14 (5.4)	6 (5.3)		5 (3.1)	4 (3.7)	1 (1.9)		
N 分期				0.193				0.729	0.861
0	60 (16.1)	38 (14.7)	22 (19.3)		24 (14.9)	15 (14.0)	9 (16.7)		
1	65 (17.4)	52 (20.1)	13 (11.4)		33 (20.5)	24 (22.4)	9 (16.7)		
2	197 (52.8)	135 (52.1)	62 (54.4)		82 (50.9)	55 (51.4)	27 (50.0)		
3	51 (13.7)	34 (13.1)	17 (14.9)		22 (13.7)	13 (12.2)	9 (16.7)		
ER 状态				<0.001				<0.001	0.707
阳性	258 (69.2)	205 (79.1)	53 (46.5)		108 (67.1)	86 (80.4)	22 (40.7)		
阴性	115 (30.8)	54 (20.9)	61 (53.5)		53 (32.9)	21 (19.6)	32 (59.3)		
PR 状态				<0.001				<0.001	0.774
阳性	229 (61.4)	187 (72.2)	42 (36.8)		96 (59.6)	75 (70.1)	21 (38.9)		
阴性	144 (38.6)	72 (27.8)	72 (63.2)		65 (40.4)	32 (29.9)	33 (61.1)		
HER-2 状态				<0.001				<0.001	0.636
阳性	150 (40.2)	70 (27.0)	80 (70.2)		69 (42.9)	28 (26.2)	41 (75.9)		
阴性	223 (59.8)	189 (73.0)	34 (29.8)		92 (57.1)	79 (73.8)	13 (24.1)		
淋巴结状态				0.333				0.833	0.831
转移	313 (83.9)	221 (85.3)	92 (80.7)		137 (85.1)	92 (86.0)	45 (83.3)		
未转移	60 (16.1)	38 (14.7)	22 (19.3)		24 (14.9)	15 (14.0)	9 (16.7)		

*各队列内 pCR 组与非 pCR 组之间比较的 P 值; †训练集与验证集之间比较的 P 值, 用于验证两个队列间的基线均衡性。

3.2. 特征选择及模型构建

从瘤内及瘤内联合瘤周 3 mm 范围中各提取了 1197 个特征, 涵盖一阶特征(n = 234)、GLCM (n = 286)、GLDM (n = 182)、GLRLM (n = 208)、GLSZM (n = 208)、NGLDM (n = 65)及形状特征(n = 14)。特征筛选流程如下: 经 t 检验或 Mann-Whitney U 检验初步筛选, 再通过 Spearman 相关性分析去除冗余, 显著降低了特征空间的维度与共线性。对于核心特征提取, 应用 LASSO 回归(图 3), 最终为各模型确定了关键特征(图 4、表 3)。这些特征保持了模型的简约性与泛化能力。

3.3. 多算法比较确定最优模型

本研究采用四种机器学习算法对不同模型的预测性能逐一评估(表 4、图 5): 在所有算法中, 瘤内联

合瘤周 3 mm 模型的 AUC 均优于单纯瘤内模型。具体而言, 在验证集中, 瘤内模型采用 RF 算法时 AUC 最高, 为 0.840 (95% CI: 0.779~0.901); 采用 XGBoost 算法时 AUC 最低, 为 0.807 (95% CI: 0.737~0.877)。与之相对, 联合模型在上述两种算法下的 AUC 分别为 0.851 (95% CI: 0.792~0.910)与 0.847 (95% CI: 0.786~0.907)。在表现相对稳定的 RF 算法中, 联合模型的准确率、敏感度及 F1 分数分别为 0.801、0.804、0.729, 均优于单纯瘤内模型。同样, 在 XGBoost 算法中, 联合模型的准确率、敏感度、特异度及 F1 分数分别为 0.801、0.778、0.813、0.724, 均优于单纯瘤内模型。

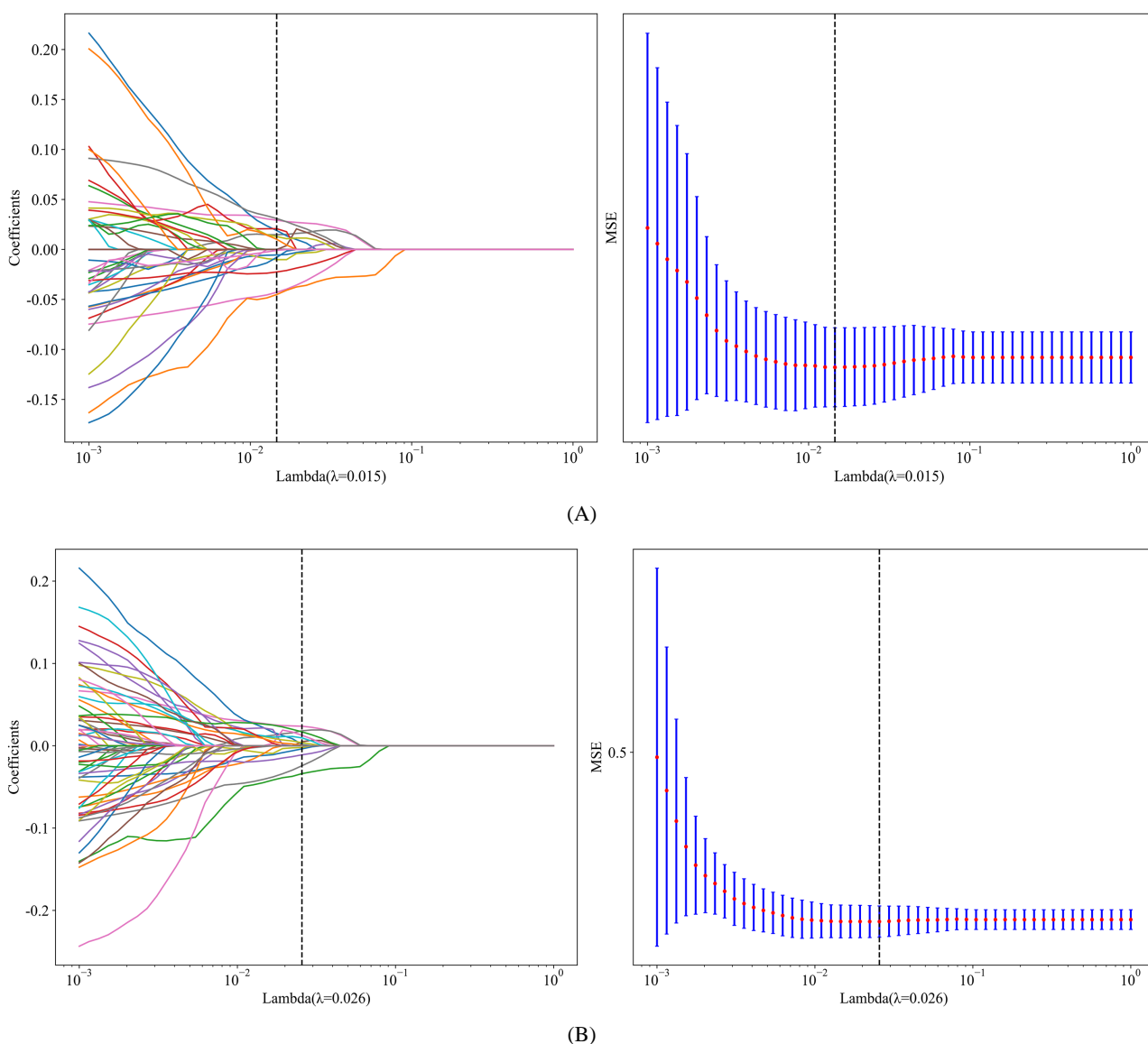


Figure 3. LASSO coefficient trajectory plot of radiomic and deep learning features and cross-validation mean squared error (MSE) curve of LASSO regression under 10-fold cross-validation. Each curve represents the trajectory of the regression coefficient for a single feature as a function of $\log(\lambda)$. The vertical dashed line indicates the optimal λ value determined by the minimum criterion, the red dashed line marks the MSE corresponding to the optimal λ value, and the blue vertical bars represent the confidence intervals for the MSE estimates. (A) Intratumoral features, $\lambda = 0.015$; (B) Intratumoral plus 3-mm peritumoral features, $\lambda = 0.026$

图 3. 10 折交叉验证下影像组学特征的 LASSO 系数轨迹图以及 LASSO 回归的交叉验证均方误差(MSE)曲线。每条曲线代表一个特征的回归系数随 $\log(\lambda)$ 变化的轨迹, 垂直虚线为最小准则下确定的最优 λ 值, 红色虚线标记最优 λ 值对应的 MSE, 蓝色竖条为 MSE 估计的置信区间。(A) 瘤内特征, $\lambda = 0.015$; (B) 瘤内 + 瘤周 3 mm 特征, $\lambda = 0.026$

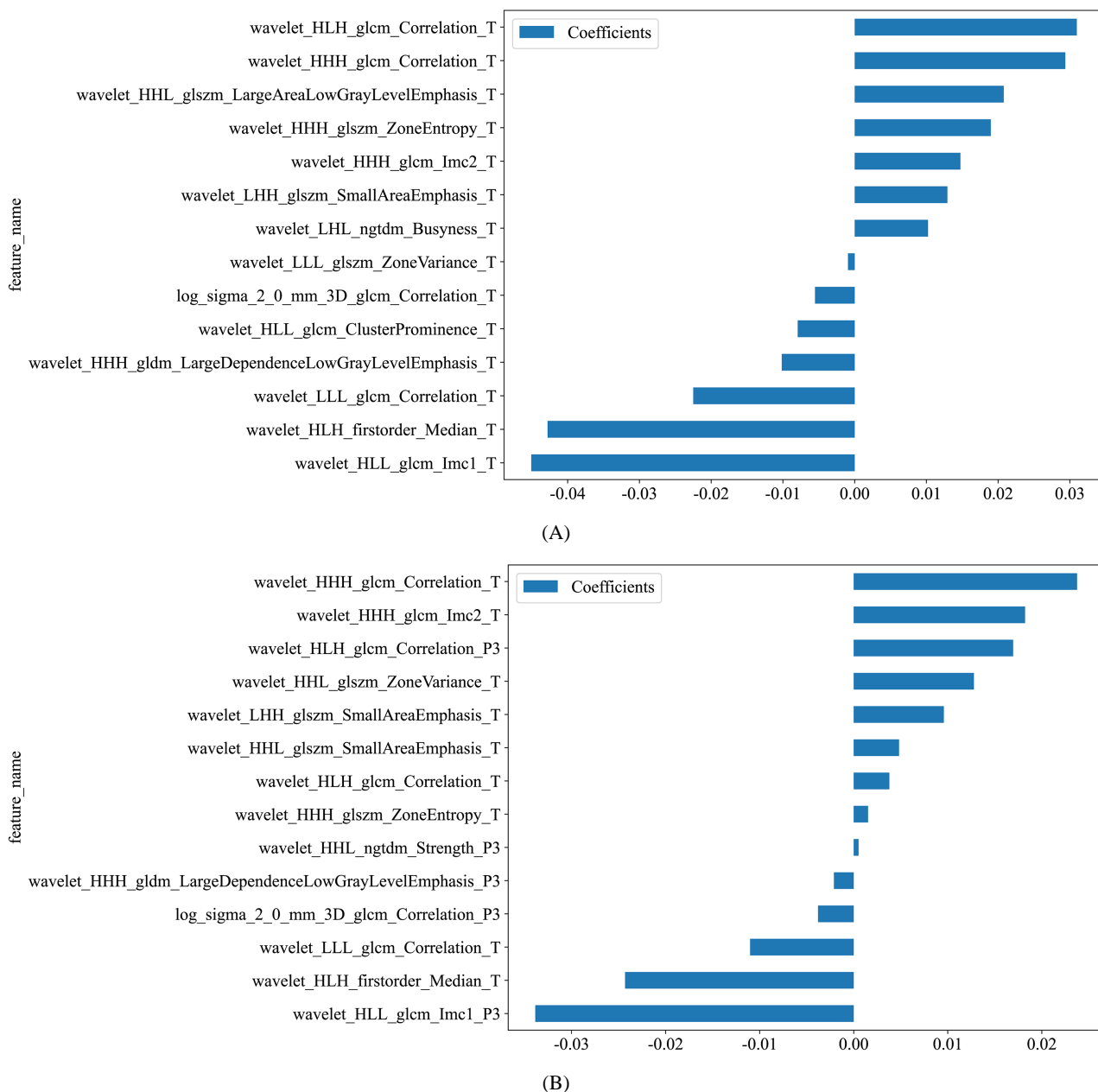


Figure 4. Radiomic features with non-zero coefficients retained by LASSO at the selected λ . The bar plot shows the (standardized) regression coefficients, with positive and negative values indicating the direction of association, respectively. (A) Intratumoral features; (B) Intratumoral plus 3-mm peritumoral features

图 4. 在所选 λ 下由 LASSO 保留的系数非零放射组学特征。柱形图表示(标准化)回归系数, 正负值分别代表关联方向。(A) 瘤内特征; (B) 瘤内 + 瘤周 3 mm 特征

Table 3. Radiomics features with non-zero coefficients retained by LASSO at the selected λ and their corresponding coefficients
表 3. 在所选 λ 下由 LASSO 保留的系数非零放射组学特征及其系数

特征集	图像滤波器	特征类型	特征名称	系数
	Log sigma 2.0 mm 3D	GLCM	Correlation	-0.006
Tumor	Wavelet-HHH	GLCM	Correlation	+0.029
	Wavelet-HHH	GLCM	Imc2	+0.015

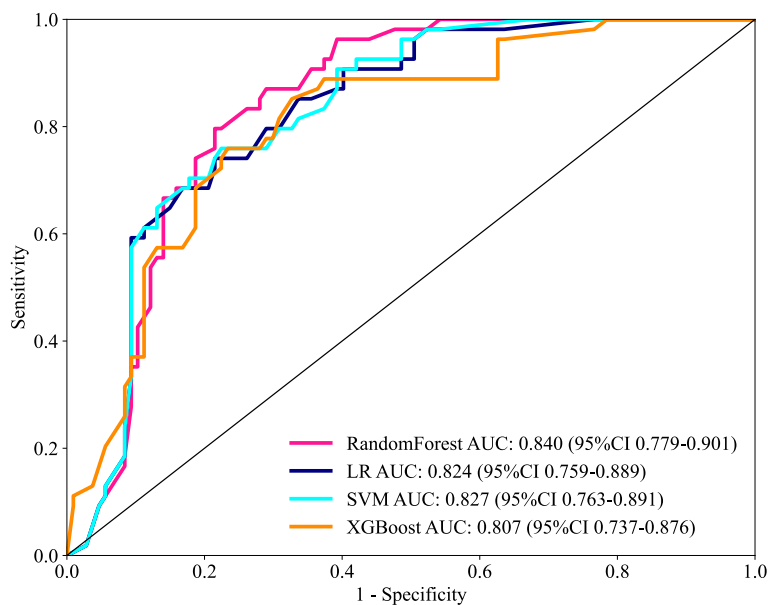
续表

	Wavelet-HHH	GLDM	Large Dependence Low Gray Level Emphasis	-0.010
	Wavelet-HHH	GLSZM	Zone Entropy	+0.019
	Wavelet-HHL	GLSZM	Large Area Low Gray Level Emphasis	+0.021
	Wavelet-HLH	First order	Median	-0.043
	Wavelet-HLH	GLCM	Correlation	+0.031
	Wavelet-HLL	GLCM	Cluster Prominence	-0.008
	Wavelet-HLL	GLCM	Imc1	-0.045
	Wavelet-LHH	GLSZM	Small Area Emphasis	+0.013
	Wavelet-LHL	NGLDM	Busyness	+0.010
	Wavelet-LLL	GLCM	Correlation	-0.023
	Wavelet-LLL	GLSZM	Zone Variance	-0.001
	Log sigma 2.0 mm 3D	GLCM	Correlation	-0.004
	Wavelet-HHH	GLCM	Correlation	+0.024
	Wavelet-HHH	GLCM	Imc2	+0.018
	Wavelet-HHH	GLDM	Large Dependence Low Gray Level Emphasis	-0.002
	Wavelet-HHH	GLSZM	Zone Entropy	+0.002
	Wavelet-HHL	GLSZM	Small Area Emphasis	+0.005
	Wavelet-HHL	GLSZM	Zone Variance	+0.012
TP3	Wavelet-HLH	First order	Median	-0.024
	Wavelet-HLH	GLCM	Correlation	+0.004
	Wavelet-HLL	GLCM	Imc1	-0.034
	Wavelet-LHH	GLSZM	Small Area Emphasis	+0.010
	Wavelet-LLL	GLCM	Correlation	-0.011
	Wavelet-HHL	NGLDM	Strength	+0.001
	Wavelet-HLH	GLCM	Correlation	+0.017

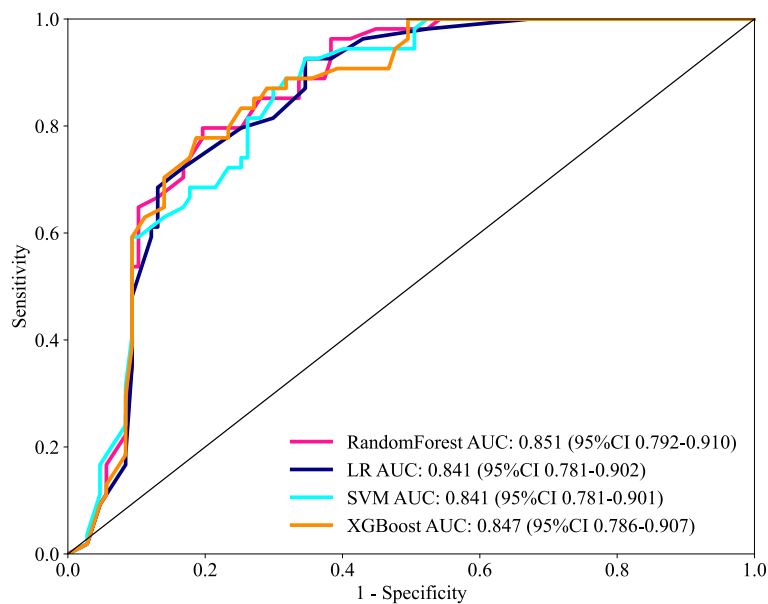
Table 4. Comparison of predictive performance of machine learning models based on feature sets from different regions in the test set

表 4. 基于不同区域特征集的机器学习模型在验证集上的预测性能比较

特征集	模型	AUC	95% CI	准确率	敏感度	特异度	F1 分数
Model-T	RF	0.840	0.779~0.901	0.789	0.796	0.785	0.717
	LR	0.824	0.759~0.889	0.770	0.741	0.785	0.684
	SVM	0.827	0.764~0.891	0.770	0.759	0.776	0.689
	XGBoost	0.807	0.737~0.877	0.764	0.759	0.766	0.683
Model-TP3	RF	0.851	0.792~0.910	0.801	0.796	0.804	0.729
	LR	0.841	0.781~0.902	0.745	0.926	0.654	0.709
	SVM	0.841	0.781~0.901	0.745	0.926	0.654	0.709
	XGBoost	0.847	0.786~0.907	0.801	0.778	0.813	0.724



(A)



(B)

Figure 5. Comparison of ROC curves of machine learning models based on feature sets from different regions in the test set. (A) Single intratumoral model; (B) Intratumoral plus 3-mm peritumoral model

图 5. 基于不同区域特征集的机器学习模型在验证集上的 ROC 曲线比较。(A) 单纯瘤内模型; (B) 瘤内 + 瘤周 3 mm 模型

3.4. 性能评估

校准曲线如图 6 所示。在验证集中，XGBoost 模型的预测概率与实际阳性事件发生概率高度吻合，校准表现最优；LR 模型校准表现良好，仅低预测概率区间存在轻微高估；RF 模型存在轻微高估偏差；SVM 模型在低预测概率区间存在明显的风险低估，校准表现较差。

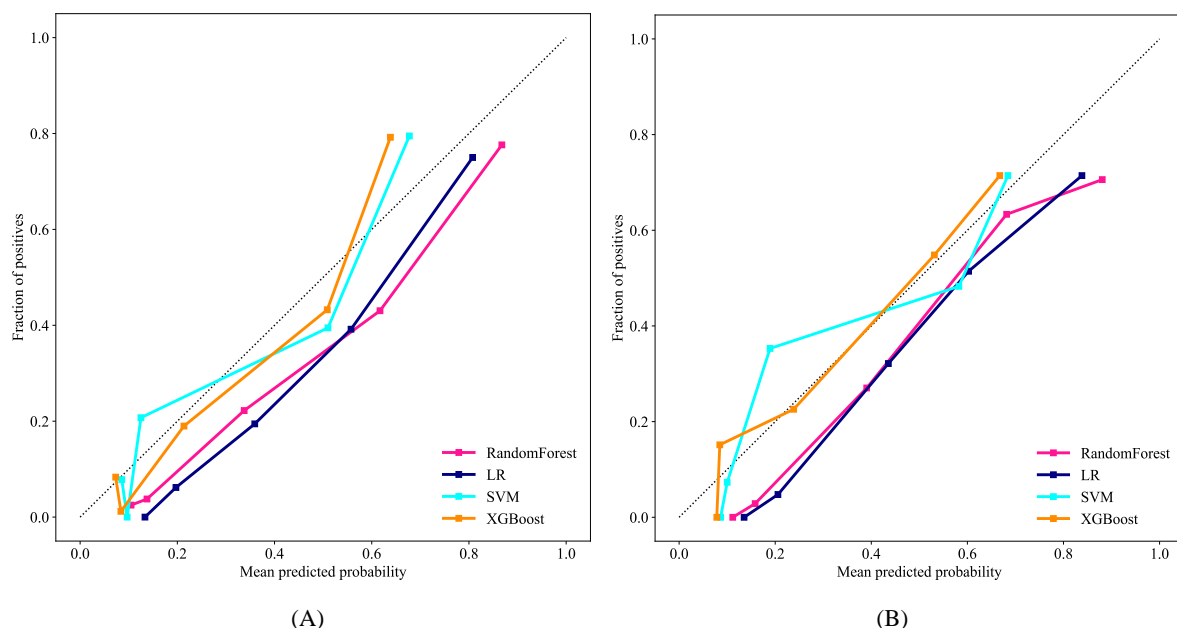


Figure 6. Calibration curves of the model in (A) training set and (B) validation set. The horizontal axis represents the predicted probability, and the vertical axis represents the actual observed incidence of outcomes. The 45° diagonal line indicates ideal calibration. The closer the calibration curve is to the diagonal line, the better the calibration performance of the model

图 6. 模型在(A)训练集和(B)验证集上的校准曲线。横轴为预测概率, 纵轴为实际观察到的结局发生频率; 45°对角线表示理想校准, 校准曲线越接近对角线, 模型校准度越好

DCA 结果(图 7)显示, RF、LR、SVM 及 XGBoost 模型的净获益曲线均高于“全干预”和“不干预”两条参考线, 在阈值概率 0%~80%的范围内, 使用上述模型指导临床决策, 均能为患者带来优于常规策略的净获益, 提示模型具备良好的临床实用价值。其中, RF 与 LR 模型在中高阈值概率区间的净获益更稳定, 临床适用性更广。

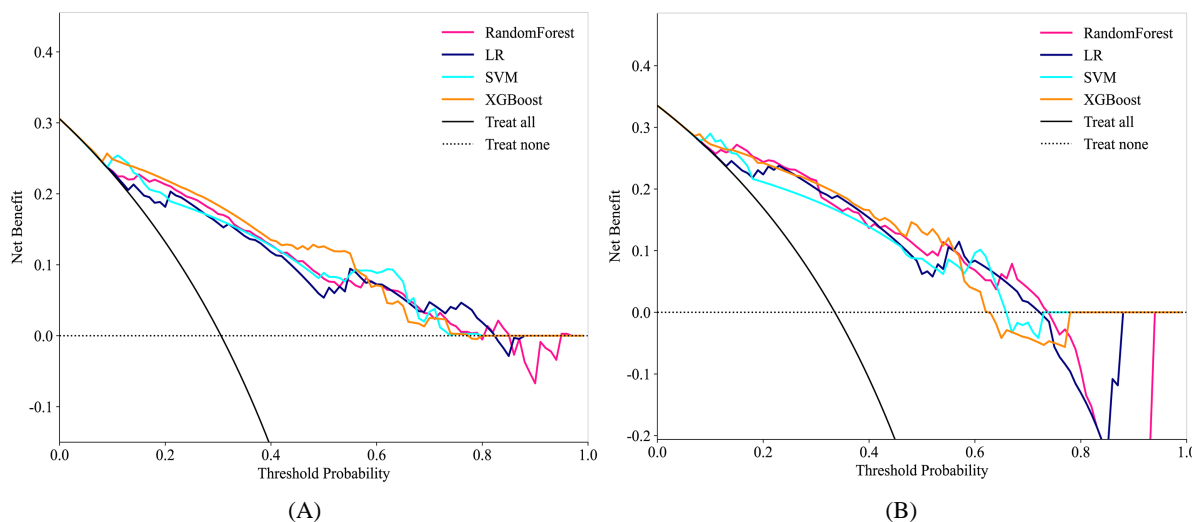


Figure 7. Decision curves of the model in (A) training set and (B) validation set. Decision curve analysis was applied to compare the net benefit of the model within different threshold probabilities in the training set (A) and validation set (B). The “Treat-all” and “Treat-none” strategies are presented as reference lines

图 7. 模型在(A)训练集以及(B)验证集中的决策曲线。决策曲线分析比较模型在(A)训练集与(B)验证集中不同阈值概率范围内的净获益; “Treat-all (全部干预)”与“Treat-none (不干预)”策略作为参考线展示

4. 讨论

pCR 是乳腺癌新辅助治疗疗效与长期预后的关键替代终点,尤其在 HER-2 阳性及三阴性亚型中提示良好预后[2] [3]。精准预测 pCR 有助于优化临床决策:获益概率高的患者可考虑降阶辅助治疗,而获益概率低者可及时更换方案,避免毒性反应与治疗延误。乳腺癌高度异质性导致患者对 NST 的反应存在显著个体差异。传统影像学仅依赖形态学评估,易出现假性进展并导致临床决策延迟。因此,治疗前无创预测 pCR 具有重要临床价值。本研究构建的影像组学联合模型表现优异,验证集最优 AUC 为 0.851 (95% CI: 0.792~0.910),效能优于单一瘤内模型。这表明该范围可能最有效捕捉与血管生成、免疫浸润、基质重塑、水肿及炎症相关的生物学信号[28] [29],印证了瘤内异质性与瘤周微环境整合建模的科学合理性:瘤内特征聚焦肿瘤本体的异质性刻画,瘤周特征则从微环境角度捕捉肿瘤的侵袭性信号,二者信息互补显著增强了预测效能。

瘤周区域在肿瘤发生、进展及治疗反应中具有重要的生物学意义。它并非被动的“空白区域”,而是富含免疫反应、血管生成及基质重塑相关信息的生物学活性区域。既往研究(如 Braman 等[24] [25])已证实,瘤周影像组学特征与肿瘤浸润淋巴细胞密度相关,并可预测乳腺癌的治疗反应。Li 等[30]进一步指出,瘤内联合瘤周 10 mm 模型的 AUC 优于单区域模型。然而,关于最优瘤周宽度尚未达成共识。未来可在独立队列中进行更精细的探索(如 1 mm 梯度)。

本研究还对比了 LR、RF、SVM 与 XGBoost 四种算法,不同算法基于不同的数学原理,通过多算法对比可避免单一算法的偶然性结果,证明预测效能源于数据中真实存在的规律,提升模型稳健性、适配数据特性、增强方法学严谨性。

针对联合模型所筛选出的 14 个特征,本研究从变换类型、特征类别及空间位置三个维度进行了分析。在变换类型方面,小波特征占总特征数的 92.90% (13/14) (表 3)。这一高占比归因于小波变换具备优异的时频局部化能力,其可提取多尺度的边缘与纹理信息,对肿瘤异质性具有较高的敏感性[31] [32]。Zhou 等[33]的研究亦证实,相较于单纯的体积或边缘纹理特征,经小波变换处理的纹理特征在评估局部晚期乳腺癌 NST 疗效时具有更优的预测效能。在特征类别方面,模型选取了 13 个纹理特征,可灵敏地反映微环境变化,例如血管生成与基质重塑过程[24] [25] [34]。在空间分布上,这些特征包含 9 个瘤内标志物与 5 个瘤周标志物(图 4)。具体而言,瘤周特征(Wavelet_HLL_GLCM_IMC1_P3)系数最大且与 pCR 负相关,提示非 pCR 病灶外纹理更趋复杂,进一步表明瘤周区域所携带的微环境信息对 pCR 预测具有重要价值。

本研究最主要的局限性在于采用单中心回顾性设计且缺乏独立的外部验证。尽管验证集在特征筛选与模型训练过程中被严格划分,但由于训练集与验证集均来源于同一医疗机构,使用相同的 3.0 T GE Signa HDxt MRI 扫描,且患者人群具有同源性,因此本研究报告的 AUC 可能高估了模型在不同磁共振品牌、扫描参数及不同人群中的实际泛化能力。同时,影像采集设备与参数的差异极易导致数据异质性。此外,目前整个影像组学流程(包括 ROI 分割与特征提取)尚未形成统一的标准方案,这一缺陷可能引入技术性变异。同时,高维组学特征与肿瘤潜在生物学特性之间的关联仍不明确,阻碍了临床医生对预测结果的解读与信任。本研究设计聚焦于比较单纯瘤内与瘤内联合瘤周 3 mm 影像组学模型的诊断效能,为控制混杂因素、单纯评估瘤周影像信息的增量价值,未引入临床基线及病理相关预测因子进行联合建模分析,失去了强预测变量,模型的效能上限和区分度受限。最后,本研究仅依赖单一 MRI 序列,这使得模型无法全面刻画肿瘤多维度、跨尺度的复杂生物学行为。

未来研究可通过多种策略提升乳腺癌新辅助治疗反应预测的准确性与临床应用价值。针对上述泛化性不足的问题,可与利用不同磁共振(如西门子、飞利浦)的医疗机构开展多中心合作并纳入临床预测指

标, 前瞻性评估模型的迁移能力, 并将公开本研究的特征提取流程, 为独立外部验证提供便利。除外部验证外, 未来还可引入模型可视化技术提升可解释性, 整合多参数 MRI、病理切片及多组学数据构建更稳健的预测模型[35]-[42], 同时还可以探讨多梯度瘤周边界对预测效能的影响, 可将瘤周区域进一步划分为近瘤周区、远瘤周区, 或按肿瘤象限、浸润前沿进行非对称分区, 探究不同解剖亚区瘤周影像特征的增量价值, 明确肿瘤微环境不同圈层的影像异质性差异。后续可将最优瘤周范围提取的影像组学特征, 与术后病理瘤周淋巴细胞浸润、血管生成[28]、间质增生、肿瘤浸润程度等病理指标进行相关性分析, 从生物学机制层面解释为何特定瘤周范围具备额外预测价值, 提升模型的生物学可解释性。

5. 结论

本研究初步证实, 瘤周区域对预测乳腺癌新辅助治疗后的病理完全缓解率具有额外价值。本研究构建的联合模型融合了瘤内及瘤周影像组学特征, 在验证集中实现 AUC 0.851 (95% CI: 0.792~0.910), 显著优于单一瘤内模型。该模型在鉴别效能、校准度及决策曲线净获益三方面均表现优异, 多项互补指标共同印证其可靠性。鉴于本研究为单中心、单平台设计, 上述结果仍需在前瞻性、多中心队列中开展外部验证, 方可进一步推向临床应用。若未来得以验证, 该模型有望为新辅助治疗人群分层及个体化手术方案制定提供客观、无创的参考依据。

声明

本研究经青岛大学附属医院伦理委员会批准(伦理号: QYFYWZLL42167), 可免除患者知情同意。

参考文献

- [1] Bray, F., Laversanne, M., Sung, H., Ferlay, J., Siegel, R.L., Soerjomataram, I., *et al.* (2024) Global Cancer Statistics 2022: GLOBOCAN Estimates of Incidence and Mortality Worldwide for 36 Cancers in 185 Countries. *CA: A Cancer Journal for Clinicians*, **74**, 229-263. <https://doi.org/10.3322/caac.21834>
- [2] Cortazar, P., Zhang, L., Untch, M., Mehta, K., Costantino, J.P., Wolmark, N., *et al.* (2014) Pathological Complete Response and Long-Term Clinical Benefit in Breast Cancer: The CTNeoBC Pooled Analysis. *The Lancet*, **384**, 164-172. [https://doi.org/10.1016/s0140-6736\(13\)62422-8](https://doi.org/10.1016/s0140-6736(13)62422-8)
- [3] Yee, D., DeMichele, A.M., Yau, C., Isaacs, C., Symmans, W.F., Albain, K.S., *et al.* (2020) Association of Event-Free and Distant Recurrence-Free Survival with Individual-Level Pathologic Complete Response in Neoadjuvant Treatment of Stages 2 and 3 Breast Cancer: Three-Year Follow-Up Analysis for the I-SPY2 Adaptively Randomized Clinical Trial. *JAMA Oncology*, **6**, 1355-1362. <https://doi.org/10.1001/jamaoncol.2020.2535>
- [4] Romeo, V., Accardo, G., Perillo, T., Basso, L., Garbino, N., Nicolai, E., *et al.* (2021) Assessment and Prediction of Response to Neoadjuvant Chemotherapy in Breast Cancer: A Comparison of Imaging Modalities and Future Perspectives. *Cancers*, **13**, Article 3521. <https://doi.org/10.3390/cancers13143521>
- [5] Leong, K.M., Lau, P. and Ramadan, S. (2015) Utilisation of MR Spectroscopy and Diffusion Weighted Imaging in Predicting and Monitoring of Breast Cancer Response to Chemotherapy. *Journal of Medical Imaging and Radiation Oncology*, **59**, 268-277. <https://doi.org/10.1111/1754-9485.12310>
- [6] Lambin, P., Rios-Velazquez, E., Leijenaar, R., Carvalho, S., van Stiphout, R.G.P.M., Granton, P., *et al.* (2012) Radiomics: Extracting More Information from Medical Images Using Advanced Feature Analysis. *European Journal of Cancer*, **48**, 441-446. <https://doi.org/10.1016/j.ejca.2011.11.036>
- [7] Daimiel Naranjo, I., Gibbs, P., Reiner, J.S., Lo Gullo, R., Sooknanan, C., Thakur, S.B., *et al.* (2021) Radiomics and Machine Learning with Multiparametric Breast MRI for Improved Diagnostic Accuracy in Breast Cancer Diagnosis. *Diagnostics*, **11**, Article 919. <https://doi.org/10.3390/diagnostics11060919>
- [8] Zhang, R., Wei, W., Li, R., Li, J., Zhou, Z., Ma, M., *et al.* (2022) An MRI-Based Radiomics Model for Predicting the Benignity and Malignancy of BI-RADS 4 Breast Lesions. *Frontiers in Oncology*, **11**, Article 733260. <https://doi.org/10.3389/fonc.2021.733260>
- [9] Zhang, J., Zhan, C., Zhang, C., Song, Y., Yan, X., Guo, Y., *et al.* (2023) Fully Automatic Classification of Breast Lesions on Multi-Parameter MRI Using a Radiomics Model with Minimal Number of Stable, Interpretable Features. *La radiologia medica*, **128**, 160-170. <https://doi.org/10.1007/s11547-023-01594-w>

- [10] Li, H., Zhu, Y., Burnside, E.S., Huang, E., Drukker, K., Hoadley, K.A., *et al.* (2016) Quantitative MRI Radiomics in the Prediction of Molecular Classifications of Breast Cancer Subtypes in the TCGA/TCIA Data Set. *NPJ Breast Cancer*, **2**, Article No. 16012. <https://doi.org/10.1038/nnpjbcancer.2016.12>
- [11] Leithner, D., Horvat, J.V., Marino, M.A., Bernard-Davila, B., Jochelson, M.S., Ochoa-Albiztegui, R.E., *et al.* (2019) Radiomic Signatures with Contrast-Enhanced Magnetic Resonance Imaging for the Assessment of Breast Cancer Receptor Status and Molecular Subtypes: Initial Results. *Breast Cancer Research*, **21**, Article No. 106. <https://doi.org/10.1186/s13058-019-1187-z>
- [12] Han, L., Zhu, Y., Liu, Z., Yu, T., He, C., Jiang, W., *et al.* (2019) Radiomic Nomogram for Prediction of Axillary Lymph Node Metastasis in Breast Cancer. *European Radiology*, **29**, 3820-3829. <https://doi.org/10.1007/s00330-018-5981-2>
- [13] Chen, Y., Li, J., Zhang, J., Yu, Z. and Jiang, H. (2024) Radiomic Nomogram for Predicting Axillary Lymph Node Metastasis in Patients with Breast Cancer. *Academic Radiology*, **31**, 788-799. <https://doi.org/10.1016/j.acra.2023.10.026>
- [14] Yu, Y., Tan, Y., Xie, C., Hu, Q., Ouyang, J., Chen, Y., *et al.* (2020) Development and Validation of a Preoperative Magnetic Resonance Imaging Radiomics-Based Signature to Predict Axillary Lymph Node Metastasis and Disease-Free Survival in Patients with Early-Stage Breast Cancer. *JAMA Network Open*, **3**, e2028086. <https://doi.org/10.1001/jamanetworkopen.2020.28086>
- [15] Guo, L., Du, S., Gao, S., Zhao, R., Huang, G., Jin, F., *et al.* (2022) Delta-Radiomics Based on Dynamic Contrast-Enhanced MRI Predicts Pathologic Complete Response in Breast Cancer Patients Treated with Neoadjuvant Chemotherapy. *Cancers*, **14**, Article 3515. <https://doi.org/10.3390/cancers14143515>
- [16] Shi, Z., Huang, X., Cheng, Z., Xu, Z., Lin, H., Liu, C., *et al.* (2023) Erratum For: MRI-Based Quantification of Intratumoral Heterogeneity for Predicting Treatment Response to Neoadjuvant Chemotherapy in Breast Cancer. *Radiology*, **308**, e222830. <https://doi.org/10.1148/radiol.239021>
- [17] Maller, O., Martinson, H. and Schedin, P. (2010) Extracellular Matrix Composition Reveals Complex and Dynamic Stromal-Epithelial Interactions in the Mammary Gland. *Journal of Mammary Gland Biology and Neoplasia*, **15**, 301-318. <https://doi.org/10.1007/s10911-010-9189-6>
- [18] Wu, J., Li, B., Sun, X., Cao, G., Rubin, D.L., Napel, S., *et al.* (2017) Heterogeneous Enhancement Patterns of Tumor-Adjacent Parenchyma at MR Imaging Are Associated with Dysregulated Signaling Pathways and Poor Survival in Breast Cancer. *Radiology*, **285**, 401-413. <https://doi.org/10.1148/radiol.2017162823>
- [19] Hoffmann, E., Masthoff, M., Kunz, W.G., Seidensticker, M., Bobe, S., Gerwing, M., *et al.* (2024) Multiparametric MRI for Characterization of the Tumour Microenvironment. *Nature Reviews Clinical Oncology*, **21**, 428-448. <https://doi.org/10.1038/s41571-024-00891-1>
- [20] Hammond, M.E.H., Hayes, D.F., Dowsett, M., Allred, D.C., Hagerty, K.L., Badve, S., *et al.* (2010) American Society of Clinical Oncology/College of American Pathologists Guideline Recommendations for Immunohistochemical Testing of Estrogen and Progesterone Receptors in Breast Cancer. *Journal of Clinical Oncology*, **28**, 2784-2795. <https://doi.org/10.1200/jco.2009.25.6529>
- [21] Wolff, A.C., Hammond, M.E.H., Hicks, D.G., Dowsett, M., McShane, L.M., Allison, K.H., *et al.* (2013) Recommendations for Human Epidermal Growth Factor Receptor 2 Testing in Breast Cancer: American Society of Clinical Oncology/College of American Pathologists Clinical Practice Guideline Update. *Journal of Clinical Oncology*, **31**, 3997-4013. <https://doi.org/10.1200/jco.2013.50.9984>
- [22] Liu, Z., Wang, S., Dong, D., Wei, J., Fang, C., Zhou, X., *et al.* (2019) The Applications of Radiomics in Precision Diagnosis and Treatment of Oncology: Opportunities and Challenges. *Theranostics*, **9**, 1303-1322. <https://doi.org/10.7150/thno.30309>
- [23] Satake, H., Ishigaki, S., Ito, R. and Naganawa, S. (2022) Radiomics in Breast MRI: Current Progress toward Clinical Application in the Era of Artificial Intelligence. *La radiologia medica*, **127**, 39-56. <https://doi.org/10.1007/s11547-021-01423-y>
- [24] Braman, N.M., Etesami, M., Prasanna, P., Dubchuk, C., Gilmore, H., Tiwari, P., *et al.* (2017) Intratumoral and Peritumoral Radiomics for the Pretreatment Prediction of Pathological Complete Response to Neoadjuvant Chemotherapy Based on Breast DCE-MRI. *Breast Cancer Research*, **19**, Article No. 57. <https://doi.org/10.1186/s13058-017-0846-1>
- [25] Braman, N., Prasanna, P., Whitney, J., Singh, S., Beig, N., Etesami, M., *et al.* (2019) Association of Peritumoral Radiomics with Tumor Biology and Pathologic Response to Preoperative Targeted Therapy for HER2 (ERBB2)-Positive Breast Cancer. *JAMA Network Open*, **2**, e192561. <https://doi.org/10.1001/jamanetworkopen.2019.2561>
- [26] Conti, A., Duggento, A., Indovina, I., Guerrisi, M. and Toschi, N. (2021) Radiomics in Breast Cancer Classification and Prediction. *Seminars in Cancer Biology*, **72**, 238-250. <https://doi.org/10.1016/j.semcancer.2020.04.002>
- [27] Zhang, X., Zhang, Y., Zhang, G., Qiu, X., Tan, W., Yin, X., *et al.* (2022) Deep Learning with Radiomics for Disease Diagnosis and Treatment: Challenges and Potential. *Frontiers in Oncology*, **12**, Article 773840. <https://doi.org/10.3389/fonc.2022.773840>

- [28] Xie, T., Gong, J., Zhao, Q., Wu, C., Wu, S., Peng, W., *et al.* (2024) Development and Validation of Peritumoral Vascular and Intratumoral Radiomics to Predict Pathologic Complete Responses to Neoadjuvant Chemotherapy in Patients with Triple-Negative Breast Cancer. *BMC Medical Imaging*, **24**, Article No. 136. <https://doi.org/10.1186/s12880-024-01311-7>
- [29] Tu, Y.S., Weng, A.T., Ren, A.L., *et al.* (2023) Multimodal MRI Manifestations and Pathological Basis of Peritumoral Infiltration of Glioma in Rat. *Chinese Journal of Magnetic Resonance Imaging*, **14**, 105-110.
- [30] Li, C., Lu, N., He, Z., Tan, Y., Liu, Y., Chen, Y., *et al.* (2022) A Noninvasive Tool Based on Magnetic Resonance Imaging Radiomics for the Preoperative Prediction of Pathological Complete Response to Neoadjuvant Chemotherapy in Breast Cancer. *Annals of Surgical Oncology*, **29**, 7685-7693. <https://doi.org/10.1245/s10434-022-12034-w>
- [31] Shuvo, S.B., Alam, S.S., Ayman, S.U., Chakma, A., Salvi, M., Seoni, S., *et al.* (2025) Application of Wavelet Transformation and Artificial Intelligence Techniques in Healthcare: A Systemic Review. *WIREs Data Mining and Knowledge Discovery*, **15**, e70007. <https://doi.org/10.1002/widm.70007>
- [32] Tang, V.H., Duong, S.T.M., Nguyen, C.D.T., Huynh, T.M., Duc, V.T., Phan, C., *et al.* (2023) Wavelet Radiomics Features from Multiphase CT Images for Screening Hepatocellular Carcinoma: Analysis and Comparison. *Scientific Reports*, **13**, Article No. 19559. <https://doi.org/10.1038/s41598-023-46695-8>
- [33] Zhou, J., Lu, J., Gao, C., Zeng, J., Zhou, C., Lai, X., *et al.* (2020) Predicting the Response to Neoadjuvant Chemotherapy for Breast Cancer: Wavelet Transforming Radiomics in MRI. *BMC Cancer*, **20**, Article No. 100. <https://doi.org/10.1186/s12885-020-6523-2>
- [34] Park, J., Kim, M.J., Yoon, J., Han, K., Kim, E., Sohn, J.H., *et al.* (2023) Machine Learning Predicts Pathologic Complete Response to Neoadjuvant Chemotherapy for ER + HER2- Breast Cancer: Integrating Tumoral and Peritumoral MRI Radiomic Features. *Diagnostics*, **13**, Article 3031. <https://doi.org/10.3390/diagnostics13193031>
- [35] Du, Y., Zhu, Y., Yang, M., Zhang, A., Zhang, L. and Zhou, Z. (2025) Deep Learning Model Based on DCE-MRI: Fusion of 3D Features of Tumor, Peritumoral Vessels and Metastatic Lymph Nodes for Prediction of Pathological Complete Response to Neoadjuvant Therapy in Breast Cancer. *Frontiers in Oncology*, **15**, Article 1664631. <https://doi.org/10.3389/fonc.2025.1664631>
- [36] Xu, S., Ying, Y., Hu, Q., Li, X., Li, Y., Xiong, H., *et al.* (2025) Fusion Model Integrating Multi-Sequence MRI Radiomics and Habitat Imaging for Predicting Pathological Complete Response in Breast Cancer Treated with Neoadjuvant Therapy. *Cancer Imaging*, **25**, Article No. 108. <https://doi.org/10.1186/s40644-025-00929-2>
- [37] Yuan, Q., Hong, Z., Ye, R., Yang, P., Lin, J., Jiang, X., *et al.* (2026) Integrating Deep Feature Extraction and MRI Radiomics for Survival Prediction in Breast Cancer after Neoadjuvant Chemotherapy. *Academic Radiology*, **33**, 872-888. <https://doi.org/10.1016/j.acra.2025.10.050>
- [38] Liu, J., Wang, X., Mao, N., Hua, H., Zhong, X., Han, J., *et al.* (2025) The Value of Machine Learning Based on Magnetic Resonance Imaging (MRI) and Biopsy Whole-Slide Image to Predict Pathological Complete Response to Breast Cancer after Neoadjuvant Chemotherapy: A Two-Centre Study. *Clinical Radiology*, **87**, Article ID: 106976. <https://doi.org/10.1016/j.crad.2025.106976>
- [39] Xu, N., Guo, X., Ouyang, Z., Ran, F., Li, Q., Duan, X., *et al.* (2024) Multiparametric MRI-Based Radiomics Combined with Pathomics Features for Prediction of the Efficacy of Neoadjuvant Chemotherapy in Breast Cancer. *Heliyon*, **10**, e24371. <https://doi.org/10.1016/j.heliyon.2024.e24371>
- [40] Duan, J., Zhao, Y., Sun, Q., Liang, D., Liu, Z., Chen, X., *et al.* (2023) Imaging-Proteomic Analysis for Prediction of Neoadjuvant Chemotherapy Responses in Patients with Breast Cancer. *Cancer Medicine*, **12**, 21256-21269. <https://doi.org/10.1002/cam4.6704>
- [41] Zhang, T., Zhao, L., Cui, T., Zhou, Y., Li, P., Luo, C., *et al.* (2025) Spatial-Temporal Radiogenomics in Predicting Neoadjuvant Chemotherapy Efficacy for Breast Cancer: A Comprehensive Review. *Journal of Translational Medicine*, **23**, Article No. 681. <https://doi.org/10.1186/s12967-025-06641-w>
- [42] Huang, Y., Zhu, T., Zhang, X., Li, W., Zheng, X., Cheng, M., *et al.* (2023) Longitudinal MRI-Based Fusion Novel Model Predicts Pathological Complete Response in Breast Cancer Treated with Neoadjuvant Chemotherapy: A Multicenter, Retrospective Study. *eClinicalMedicine*, **58**, Article ID: 101899. <https://doi.org/10.1016/j.eclinm.2023.101899>